Model Sensitivity during Extreme Positive and Negative Surges in the Río de la Plata Estuary: Highlighting the Need for an Appropriate Hindcast/Forecast System

MATÍAS G. DINÁPOLI

Centro de Investigaciones del Mar y la Atmósfera (CIMA/CONICET-UBA), and Instituto Franco-Argentino para el Estudio del Clima y sus Impactos (UMI IFAECI/CNRS-CONICET-UBA), Ciudad Universitaria, Ciudad Autónoma de Buenos Aires, Buenos Aires, Argentina

CLAUDIA G. SIMIONATO AND DIEGO MOREIRA

Centro de Investigaciones del Mar y la Atmósfera (CIMA/CONICET-UBA), and Instituto Franco-Argentino para el Estudio del Clima y sus Impactos (UMI IFAECI/CNRS-CONICET-UBA), Ciudad Universitaria, Ciudad Autónoma de Buenos Aires, and Departamento de Ciencias de la Atmósfera y los Océanos, FCEN, Universidad de Buenos Aires, Buenos Aires, Argentina

(Manuscript received 14 August 2019, in final form 3 April 2020)

ABSTRACT

The large and fast-flowing Río de la Plata (RdP) estuary is affected by extreme storm surges (above ±2 m with respect to tidal datum), which have large impacts on the millions of inhabitants and for navigation. In this work the Coastal and Regional Ocean Community Model (CROCO) numerical model was modified and implemented as a set of regional one-way nested 2D applications for the hindcast/forecast of water level in the RdP. A sensitivity analysis (SA) was carried out to determine the impact on the numerical solutions of the uncertainties in the different modeling parameter forcings and to highlight the need for the construction of a modeling system that provides meaningful information to the potential users. The SA included the friction coefficients, the wind speed and direction, the atmospheric surface pressure, and the continental discharge. Water level is most sensitive to uncertainties in the wind forcing; even small changes in this input can create large errors in the water level forecast/hindcast. Forcing with different analyses' wind products yielded differences of up to 50% in the peak water levels. Results also showed that the modeling system requires a reasonable adjustment of the bottom friction parameters; that it is important to include the atmospheric surface pressure forcing; and that, from the point of view of water level forecast, it is not necessary to couple a hydrological model in spite of the enormous runoff of this estuary. Given the strong sensitivity to errors in the wind forcing, we believe it is important to provide estimates of uncertainty together with hindcast/forecast water level for these predictions to be of greatest quality and practical applicability.

1. Introduction

Resulting from the confluence of the Paraná and Uruguay Rivers, the shallow Río de la Plata (RdP; Fig. 1) is one of the largest estuaries in the world (Shiklomanov 1998), constituting the second largest basin of South America after the Amazon (Meccia et al. 2009). This estuary ranks fifth worldwide in water discharge (Framinan et al. 1999), with an average of around 22 000 $m^3 s^{-1}$. This way, the runoff presents large variability on interannual time scales associated with El Niño–Southern Oscillation cycles (Robertson and Mechoso 1998), with peaks as high as 90 000 $m^3 s^{-1}$ and as low as less than 8000 $m^3 s^{-1}$ (Jaime et al. 2002). Runoff can have enormous variations on a scale of a few months.

The water level (sea surface height) in the estuary is principally characterized by the combination of a semidiurnal microtidal regimen (D'Onofrio et al. 2012) and the wind driven circulation (Simionato et al. 2004a). The latter can be explained in terms of two modes of circulation: (i) a prevailing one for winds with a cross-estuary component, related to an inflow/outflow of water at the exterior part of the RdP, and (ii) a second mode that is excited when the wind blows along the estuary axis and that has a very distinctive pattern of significant water level increase or reduction at the upper part of the estuary (Simionato et al. 2004a). A particular case of this second mode is known as *Sudestada* and is associated with strong and persistent southeasterly

Corresponding author: Matías Dinápoli, matias.dinapoli@cima.fcen.uba.ar

DOI: 10.1175/WAF-D-19-0171.1

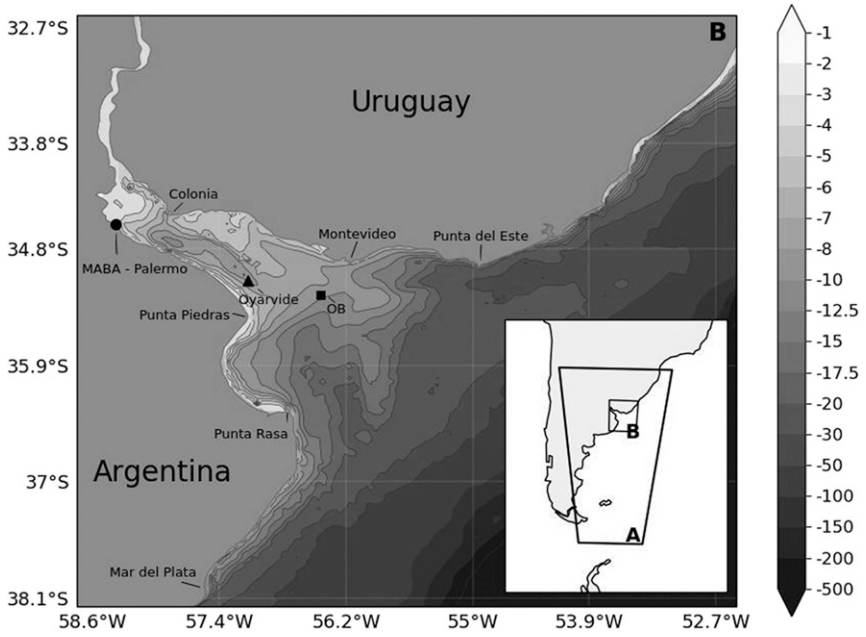

FIG. 1. Map of the study area, showing the domain of the two nested models (A and B). The isolines represent the bathymetry (m). The location of the tide gauges, Palermo (black circle) and Oyarvide (black triangle), and the oceanographic buoy (OB, black square) are also shown.

winds, which are relatively frequent in the region (Seluchi and Saulo 1998; Gan and Rao 1991). This phenomenon has historically caused catastrophic floods on the RdP coasts, threatening and claiming human lives and producing major economic and material damages (D'Onofrio et al. 1999). The Metropolitan Area of Buenos Aires City (MABA; black circle, Fig. 1), site of the capital of Argentina, with a population of more than 16 million people, is regularly affected by these events. For instance, in 2010 and 2012 extreme floods reached 2.48 and 2.30 m over tidal datum (the second maximum level during the last century) (Diario-Clarín 2010, 2012); for comparison, 1.90 m is the level of emergency alert, when people and property become in serious danger and authorities issue an alert (Balay 1961). On the other hand, negative extreme surges are associated with winds that have a dominant northwesterly component, which are less frequent in the region (D'Onofrio et al. 2008). Nevertheless, when they do occur, they inhibit the access to the principal harbours and impair the drinking water intakes for one of the most important cities of southern South America. Figure 2 shows pictures taken during different events of Sudestada (top panel) and for extreme low levels (bottom panel), illustrating the damages and difficulties occurring along the MABA coast. Even though the events are not always so extreme, they are relatively frequent, taking place several times per year; moreover, observations suggest that the number and strength of the events have been increasing with time (D'Onofrio et al. 2008; Meccia et al. 2009).

Currently, in the frame of collaborative projects between the Hydrographic Service (SHN), the National Meteorological Service (SMN), and the Centre for Atmospheric and Oceanic Research (CIMA/CONICET-UBA) of Argentina, the implementation of a storm surge hindcast/forecast model for the RdP and the adjacent continental shelf is being faced. Although during the last few years a number of high-resolution ocean global models that incorporate many ocean processes and assimilate observations have been developed at several important forecast centers of the world (e.g., HYCOM, https://www.hycom.org/hycom/overview), usually they do not take into account the tides, which can have large interaction with the surge (Wolf 1978; Idier et al. 2012). Moreover, the small details of the bathymetry (fundamental on the propagation of the surge) are not well resolved by the global general bathymetries used by those models, at least for the RdP (Saraceno et al. 2010). Therefore, if the principal goal of the numerical application is the hindcast/forecast of storm surges, it is still necessary to carry out the regionalization of a model that properly resolves those details and processes. Such a regionalization implies the development of the model architecture, making decisions about the processes and interactions to be included, and a model adjustment and validation (Kalnay 2002). Previous works have shown that the proper design of a hindcast/forecast system demands knowledge about the sources of uncertainties, the order of magnitude of the forcing effects

FIG. 2. Images from a (top) Sudestada event and (bottom) negative extreme storm surges at Buenos Aires Capital City. The top panels show how the Sudestadas overcome the defenses of the city. In opposition, the bottom panels show stranded ships during the negative case. Photos from several Argentinian newspapers.

(e.g., Bastidas et al. 2016), the relative importance of the parameters/forcings (for instance, Mayo et al. 2014; Ferreira et al. 2014; Höllt et al. 2015), the real need of their inclusion (Gayathri et al. 2019), and so on. The answer to those questions depends upon the geometry of the basin, the scale, the latitude, and the meteorological processes occurring in the region, among others (Gill 1982; Pedlosky 1987; Pugh 2004). This way, every particular area demands its own analysis (WMO 2011). In addition, the RdP is extremely wide, long, and mighty, making it hardly comparable to any other estuary in the world (Luz Clara et al. 2014). With regards to the physical processes, there is a general agreement in the scientific community that 2D barotropic models are a cost effective solution for surge hindcast/forecast (Zhang et al. 2010; WMO 2011; Idier et al. 2012). This is why even though baroclinic processes have an impact in ocean temperature and salinity, they have an almost negligible effect on the water level due to the surge (Gill 1982; Pedlosky 1987); in addition, this approach reduces the cost of the simulations and the number of parameters to be adjusted for the validation of the model.

With regards to that last step, it can be quite expensive if information about the model sensitivity to changes in the parameters and forcings of the surge is not available in advance. In addition, and for a number of different reasons, there is always some uncertainty in those parameters and forcings and which effects should be evaluated and, if necessary, quantified. Also, as a first step in the development of a hindcast/forecast model, some insight about the involved physics and interactions, and the related effect of the diverse parameters, can be very useful. In this sense, a sensitivity analysis (SA) becomes useful at this stage of the model development, because this technique permits the determination of a hierarchy of influence of the parameters/forcings on the storm surge and aids in the identification of their optimal values. Furthermore, it shows where the numerical application needs improvements contributing to further model development and allows an optimal model assembly through a reduced number of simulations (Norton 2015).

In this work, a regionalization of the numerical ocean model, the Coastal and Regional Ocean Community Model (CROCO; Debreu et al. 2012) for the RdP is carried out. This model (http://www.croco-ocean.org) has been built upon the Regional Ocean Modeling System (ROMS; Shchepetkin and McWilliams 2005) and the nonhydrostatic kernel), gradually including algorithms from Model for Applications at Regional Scales 3D (MARS3D, sediments) and HYCOM (vertical coordinates). The selection of CROCO was motivated by the fact that it is a free source code that is widely accepted and applied (e.g., Combes and Matano 2019;

Kresning et al. 2019), and that is suitable for the purpose of developing an operational system for the forecast of oceanic variables. In addition, CROCO includes the possibility of two-way interaction that can be interesting and useful in future studies (e.g., Sakamoto et al. 2019). CROCO's source code was modified to run in a 2D barotropic version. Additionally, the model was adapted to incorporate atmospheric surface pressure, which is omitted in CROCO's original version. The model was then adapted to the region in a dynamic downscaling scheme of nested models to properly model the surge, because the RdP is sensitive to atmospheric large-scale dynamics (Simionato et al. 2006), and coastally trapped waves travel to the estuary along the Argentinean coast (to the north, Southern Hemisphere). As a second step, the relative importance of the uncertainty of the diverse forcings and model parameters is studied and quantified through a SA, including the friction coefficients, the wind speed and direction, the atmospheric surface pressure, and the continental discharge. Finally, because of the scarcity of direct wind observations over the RdP estuary and the inherent limitations to the numerical modeling of winds in the area, wind uncertainties are particularly analyzed, and their propagation in the water level hindcast/forecast model solution is studied. Results are then discussed and alternative methodologies to improve the hindcast/forecast to give them truly practical utility for the users are discussed.

2. Method

a. Morris method

The sensitivity analysis applied in the work aims to establish using different analyses or methodologies (Norton 2015):

1) the relative importance or significance of the different model parameters and forcings and
2) the effect in the output value of changes (or uncertainties) in a single model parameter and/or forcing, or in a combination of them.

The SA was made following the methodology suggested by Morris (1991), which is particularly well suited for a model with significant computational overburden as is the case with CROCO in a nested scheme. This method has been widely used in problems similar to ours (e.g., Bastidas et al. 2016; Campolongo et al. 2007). In a very simplistic way, it provides a mathematical method to select a minimum number of simulations (sample) that represent a huge set of simulations (population) in a statistically correct manner. Additionally, the Morris method ranks a set of *inputs* according to their influence on the *output* of the model and highlights their nonlinearity. In this context, the inputs comprise the equations' coefficients, the model parameters, and the properties of the forcings, whereas an output is the value of a variable computed by the model or of any statistic derived from it, for example, maximum or mean values. The physical meaning stems from the variable chosen for the contrast.

The Morris methodology consists of the generation of r random *trajectories* formed by one-at-a-time perturbation of the k considered parameters. Each trajectory consists of $k + 1$ simulations; in the first one the set of parameter values is chosen randomly, and in the other k, the parameters are changed one at a time by a fixed increment or step. The step size is a fraction of the factor's range, in our case, one fourth. In the Morris method, the changes in the output due to the k changes in each single parameter for the r trajectories or realizations are treated as a sample of dimension rk. Morris suggested studying the gradient of the output in every k direction along the r trajectories. For that, he proposed to calculate the basic statistical parameters associated with the derivative of the output with respect to the inputs. If the mean of this derivative is significantly different from zero, then the input has an influence on the output. The variance determines how nonlinear is that influence. If the total number of simulations for the different values of the input were made, one could know the spreading in the solutions due to the potential changes in that input, or *sensitivity* of the model to changes in the input. Nevertheless, if the number of inputs is high, the required number of simulations would be huge and the computational cost could be excessive. For this, Morris suggested a cheap and effective computational way to get the samples for every derivative distribution. This way, the method proposes a cost effective method of evaluating the effect of the changes on the parameters with a relatively low number of simulations and much cheaper computational cost. Although different sampling schemes can be used to determine the samples, in this paper the original Morris design was followed. In order for a better intercomparison among inputs, the normalized derivative (Norton 2015) was used according to Eq. (1):

$$\frac{\partial y}{\partial p_k} \rightarrow \frac{\delta y/y}{\delta p_k/p_k} = \frac{p_k}{y}\frac{\delta y}{\delta p_k}, \tag{1}$$

where y is the output, p_k is the value of the k input, and δ is the finite difference operator.

b. Hindcast/forecast numerical model

The primitive equations CROCO model was chosen as the base for the development of a model for

the hindcast/forecast of water level at the northern Argentinean continental shelf with emphasis on the RdP estuary. Since storm surge is a barotropic process (Gill 1982; Pedlosky 1987; WMO 2011), the CROCO model was applied as a hierarchy of two one-way nested barotropic 2D models. The 2D barotropic model is based on the depth-averaged momentum and continuity equations as follows:

$$\frac{\partial \mathbf{u}}{\partial t} + (\mathbf{u}\cdot\nabla) + f\hat{\mathbf{z}}\times\mathbf{u} = -g\nabla\eta - \frac{1}{\rho_0}\nabla p_{\text{at}} + \frac{1}{\rho_0 H}(\boldsymbol{\tau}_S - \boldsymbol{\tau}_B), \tag{2}$$

$$\frac{\partial \eta}{\partial t} + \nabla\cdot(H\mathbf{u}) = 0, \tag{3}$$

where $\mathbf{u}$ represents the depth-averaged velocity; t is the time; f is the Coriolis parameter; g is the acceleration due to gravity; η is the water level; ρ_0 is the water density; p_{at} is the surface atmospheric pressure; H is the total water depth (i.e., the addition of η and the undisturbed water depth h); and $\boldsymbol{\tau}_S$ and $\boldsymbol{\tau}_B$ are the surface wind and bottom friction stresses, respectively. It was necessary to modify the source code (originally 3D) to be able to run 2D simulations; tide and runoff subcodes were modified with this aim. Besides, a subroutine was added to force the model to take into account the effect of gradients in the atmospheric surface pressure $[(1/\rho_0)\nabla p_{\text{at}}]$ that is not included in the original version of CROCO. The pre- and postprocessing routines of the model were programmed using Python, following the main ideas of object oriented programming. Data were pre- and postprocessed using "xarray" library (Hoyer and Hamman 2017) and plotted using "cartopy" (MetOffice 2015).

As above mentioned, two nested domains of different resolutions and scales were implemented to reach the RdP. Model A is the lowest resolution/largest scale spanning from 59° to 26°S and from 69° to 46°W (Fig. 1, inset), with a horizontal resolution of 7.50′ and 5.25′ in the zonal and meridional direction (equivalent to approximately 12 km), respectively. This model is used to provide boundary conditions to a higher-resolution model focused on the RdP (model B, Fig. 1). Model B covers the region between 38.20°–32.60°S and 58.75°–52.50°W. Using the empirical criteria of 1/3 reduction from father to child models (Simionato et al. 2006; Santoro et al. 2011), the horizontal resolution of model B is of 2.5′ and 1.75′ in the zonal and meridional directions (approximately 4 km), respectively. Given that the wavelength of the tide is more than 300 km (Simionato et al. 2005) and that for the surge is on the order of 1000 km (Pugh 2004), a resolution of 4 km is enough to properly solve the processes of interest and provides a reasonable number of grid points describing them throughout the entire estuary, with at least 10–12 points even at the upper part. Incrementing the resolution, in order to provide information about the details of the circulation that may occur in small inlets along the estuary or within the ports, would be desirable. Nevertheless, this will not be possible in the short term due to the lack of data of the bathymetric details in the RdP regions, except along the (narrow) navigation channels and in the vicinity and inside the main harbors. On the other hand, the aim of this work is to understand how the uncertainty in the knowledge of the parameters/forcing, and the modeling architecture affect the simulation of the dynamic processes related to tides and surges, which in turn are adequately simulated with the chosen resolution. In that sense, an increase in resolution would make the study much more expensive from the computational point of view (it should be taken into account that this work demanded hundreds of simulations) and would not change the conclusions. Bathymetries for both models were built by combining the ETOPO2v2 (NOAA 2006) dataset with data provided by the SHN for depths shallower than 200 m that come from digitization of nautical charts (SHN 1986, 1992, 1993, 1999a,b). Additionally, floodings in the RdP coast occur because rainfall cannot drain properly due to the level set by the surges; therefore overland flooding regions were not taken into account.

Model A is forced along its lateral open boundaries by the astronomical tide composed of the eight principal diurnal and semidiurnal constituents (M_2, S_2, N_2, K_2, K_1, Q_1, O_1, and P_1) provided by the TPXO9 model (Gary and Erofeeva 2002). Daily measured observations (Borús et al. 2006) are used to set the Paraná and Uruguay Rivers' runoffs. Finally, as was suggested by Simionato et al. (2006), both models are forced at the surface by wind stress and atmospheric surface pressure.

The time steps of the father and child models were 15 and 5 s, respectively, consistent with the CFL condition (Courant et al. 1928). The bottom friction coefficient is considered constant at every node of both domains and lateral friction was set to zero (see next subsection for further discussion on this issue). Finally, the model solutions were saved with 1-h time resolution for further analysis.

c. SA parameters

Since the Morris method requires a scalar output, the root-mean-square error (RMSE) was chosen. This statistic was calculated with respect to the storm surge observed at Palermo (MABA, upper estuary; Fig. 1, circle) and Oyarvide (outer intermediate estuary; Fig. 1, triangle) tidal stations. At those sites water level is

regularly measured by the SHN and, more importantly, they are representative of the internal and intermediate parts of the estuary, which are the most affected by the surge. Storm surge signals were obtained by low pass filtering (with a cutoff period of 30 h) the hourly water level observations. The inputs were chosen as those corresponding to the main forces in the momentum balance equation of the 2D barotropic model: the atmospheric forcing, the continental discharge and the bottom friction. In every case the range of variability of the diverse inputs was chosen to stress the importance of the associated physical processes on the generation and magnitude of the surge and the eventual problems that could rise from uncertainties on the forcings or model parameters. More specifically,

- Bottom friction: CROCO considers both a linear and a quadratic coefficient for bottom friction (c_l and c_D, respectively) through the parameterization in Eq. (4):

$$\boldsymbol{\tau}_B = \rho_0(c_l + c_D w)\mathbf{u}, \tag{4}$$

  where $\boldsymbol{\tau}$ is the bottom friction stress vector, ρ_0 is the water density, w is the current speed, and $\mathbf{u}$ is the velocity vector. Taking into account previous regional studies with numerical models (e.g., Simionato et al. 2004b; Combes and Matano 2014) we considered a range of variation between 2.0×10^{-3} and 3.0×10^{-3} for c_D. For c_l, ROMS documentation (ROMS 2005) suggests that it should be an order of magnitude smaller than c_D; thus, in order to explore its effect on the water level, we chose the interval ranging between 1.0×10^{-4} and $4.0 \times 10^{-4}\,\mathrm{m\,s^{-1}}$.
- Wind: It was decided to analyze the impact of wind speed w and direction Θ separately. The changes in wind speed were considered through a speed factor I, namely, the perturbed speed w' is $w' = Iw$. This scalar was chosen to vary between 0.75 and 1.25 (±25% in wind speed). The uncertainty on this parameter is large and cannot be chosen from literature for other sites. The election of its interval is, therefore, based on the averaged difference among several reanalyses for the region (further details are discussed in the next section). For the case of the wind direction, taking into account results of Simionato et al. (2004a) about the range of wind direction that produces the modes of circulation at the RdP, the direction was kept in an interval between −15° and 15° of the observed value. The conversion from wind vectors to wind stress (which is the final input to the model) was made using the quadratic law [Eq. (5)]:

$$\boldsymbol{\tau}_S = c_D^w \rho_A w_S \mathbf{u}_S, \tag{5}$$

  where $\boldsymbol{\tau}_S$ is the horizontal wind stress, c_D^w is the wind drag coefficient, ρ_A is the air density, $\mathbf{u}_S$ is the wind vector, and w_S is the wind speed. For the parameterization of the wind drag coefficient the expression provided by Bowden (1983), Eq. (6), was used:

$$c_D^w = \begin{cases} 1.1 \times 10^{-3}, & \text{for} \quad w_S < 5\,\mathrm{m\,s^{-1}} \\ \left(1.1 + \dfrac{2.1}{35} w_S\right) \times 10^{-3}, & \text{for} \quad w_S \geq 5\,\mathrm{m\,s^{-1}} \end{cases}. \tag{6}$$

  Recent works show that this kind of wind drag coefficient parameterization, usually applied in numerical models, can fail when the wind speed becomes extremely large, particularly when hurricane force is reached. For instance, Powell et al. (2003) found that surface momentum flux levels off as the wind speed increases above $24\,\mathrm{m\,s^{-1}}$. In the RdP, however, strong winds are very rare and wind speed is usually less than $22\,\mathrm{m\,s^{-1}}$ (Seluchi and Saulo 1998). The surge, although very high, is due to the estuary's dynamics and to the persistence of the wind rather than to extremely high wind speed (Simionato et al. 2004a). In that sense, the parameterization by Bowden (1983) can be regarded as valid for this study. The wind drag coefficient variation due to changes in wind speed is considered in the computation.
- Atmospheric surface pressure Γ: This variable was incorporated into the model code, because the original version of CROCO does not include the effect of the atmospheric surface pressure gradient (ASPG) on the surge. Therefore, it was decided to evaluate its relative importance and the need for its inclusion. For that, an attenuation factor Γ was considered for the perturbation P' so that $P' = \Gamma P$, with Γ chosen to vary from 0 to 1. This way, when $\Gamma = 0$ the ASPG is omitted, when $\Gamma = 1$ the ASPG is fully included, and in the intermediate range ASPG is underestimated.
- Continental discharge Q: Given that the range of variability of the continental discharge is very large in nature and that runoff cannot be considered as zero at the RdP, a factor λ of ±50% with respect to the mean observed values ($22\,000\,\mathrm{m^3\,s^{-1}}$) was considered (i.e., $Q' = \lambda Q$, with λ varying between 0.5 and 1.5). This broad range, which is larger than the interquartile range (Borús et al. 2006), will illustrate the effect of this parameter even if, as expected, it is small.

TABLE 1. Inputs considered for the SA and their ranges of variation.

Input	Interval	Unit
Quadratic bottom friction (c_D)	$[2.0; 3.0] \times 10^{-3}$	Dimensionless
Linear bottom friction (c_l)	$[1.0; 4.0] \times 10^{-4}$	m s^{-1}
Intensity factor (I)	[0.75; 1.25]	Dimensionless
Wind direction (Θ)	[−15; 15]	°
Atmospheric surface pressure (Γ)	[0; 1]	Dimensionless
Runoff (λ)	[0.5; 1.5]	Dimensionless

Previous studies have shown that lateral diffusion does not produce significant changes in barotropic models (e.g., Simionato et al. 2004b; Bastidas et al. 2016; Dinápoli 2016). Therefore, it was set to 0 for all simulations. Table 1 summarizes the chosen ranges for the diverse inputs.

3. Results

a. Sensitivity analyses

Overall, $r = 20$ realizations or trajectories were run; as $k = 6$ parameters were analyzed, $r(k + 1) = 140$ simulations were carried out. The number of 20 realizations was chosen because statistical scores stabilized after 15. The simulations were run for the late winter/spring 2010 (from 1 August to 1 December); during this period both extreme modes of oscillation were naturally excited, and water levels reached both extreme positive and negative values (Fig. 3). On September 2010, a cyclogenesis developed over Patagonia, producing strong and persistent southeasterly winds over the RdP (Fig. 3, top-left panel) that flooded the upper part of the estuary during a Sudestada (Fig. 3, bottom-left panel). On October of the same year, persistent westerly winds blew over the RdP (Fig. 3, top-right panel) activating the longitudinal mode of oscillation (Simionato et al. 2004a) that strongly reduces the water level along the Argentinean coast and floods the Uruguayan one (Fig. 3, bottom-right panel). The chosen period allows an assessment of whether the model presents different SAs for positive and negative storm surges (PSS and NSS, respectively), as well as for the full period (FP).

The set of nested models was then run for every of the 140 cases for 122 days. The first 15 days were discarded because they correspond to the spinup of the model (Dinápoli 2016); another 12.5 days were lost by the low

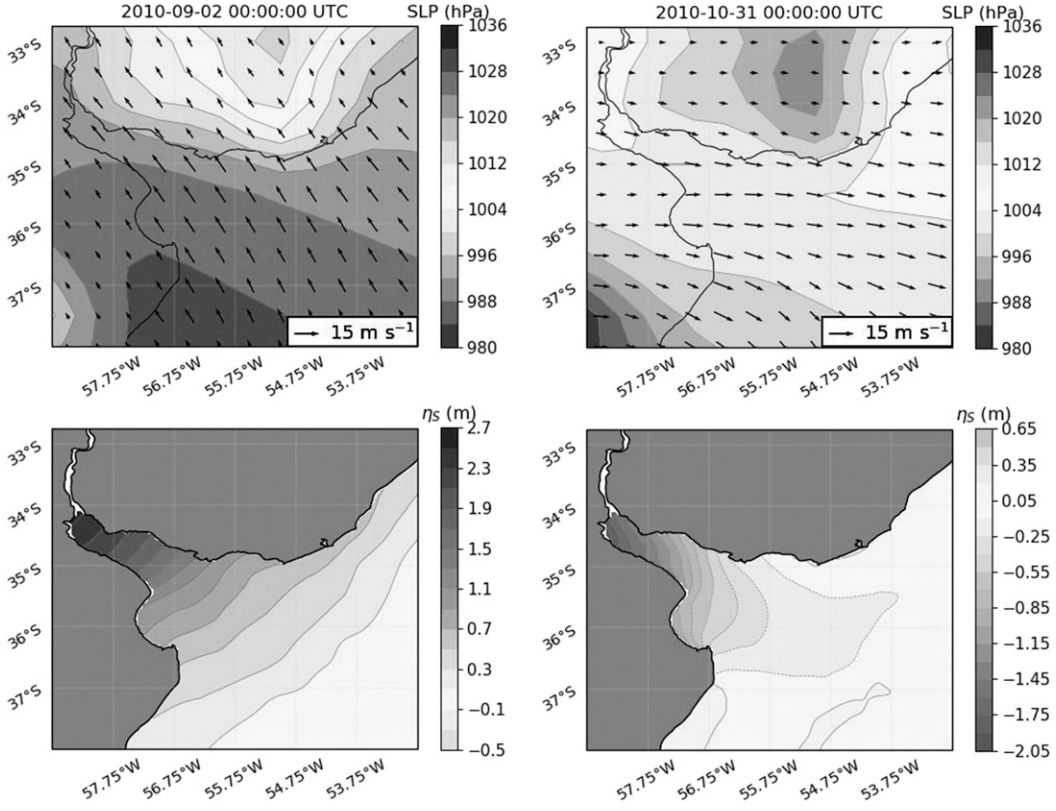

FIG. 3. (top) Synoptic conditions for (left) a Sudestada and (right) an extreme negative storm surge in September and October 2010, respectively. The isolines represent the sea level pressure (hPa) and vectors represent the wind field. (bottom) Water level for each event; the level is in meters.

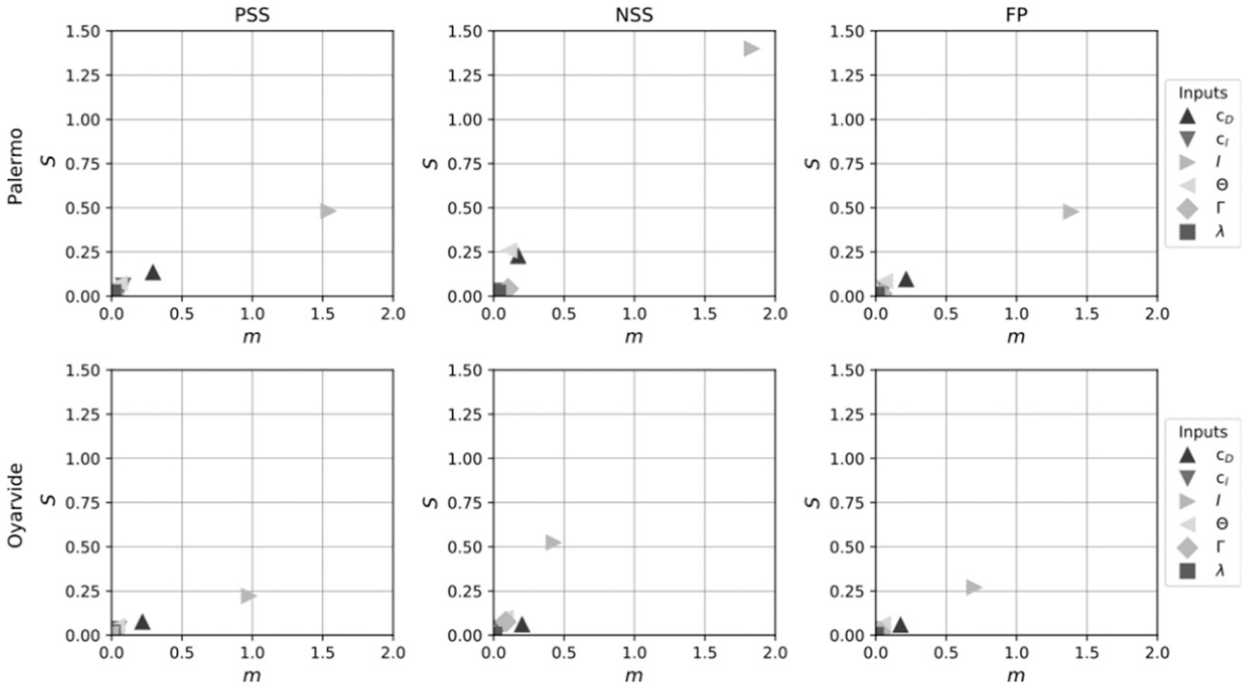

FIG. 4. Estimated means m and standard deviation S for (top) Palermo and (bottom) Oyarvide stations for the (left) positive storm surge (PSS), (center) negative storm surge (NSS), and (right) the full period (FP). All inputs are significantly different from zero according to the Morris (1991) method.

pass filtering of the series to eliminate the tide (6.25 days at both extremes of the time series). Therefore, 94.5 days were available for the analysis.

To ensure that the conclusions derived from the SA are independent of the wind data source and their eventual differences, the simulations and the corresponding SA analyses were repeated for two different wind forcing data: ERA-Interim (ERAI; Dee et al. 2011) and ERA5 (Copernicus Climate Change Service C3S 2017) of the European Centre for Medium-Range Weather Forecast (ECMWF). The models used to compute these reanalyses differ in both the involved physics and the spatial temporal resolution (see the following subsection for further details on this issue). Both reanalyses drove to the same conclusions regarding the impact and hierarchy of importance of the model inputs on the output; therefore only those corresponding to ERAI will be discussed in what follows.

The mean of every derivative distribution m was calculated as suggested by Campolongo et al. (2007), by computing the mean of the absolute values of the derivative distribution. In addition, the statistical significance of every m was tested as proposed by Morris (1991), checking that they are significantly different from zero. Figure 4 shows the mean m versus the standard deviation S of the derivative distribution function for every input at the Palermo (top panel) and Oyarvide (bottom panel) stations for every subperiod: PSS (left), NSS (center), and FP (right). The mean m was significantly different from zero for all the inputs, indicating that their uncertainty has a nonnull influence on the model solution (water level). Qualitatively, every event and station display a similar $m - S$ scatterplot pattern. The uncertainty on the wind speed I is, by far, the most influencing and this input has nonlinearity; the uncertainty in all the other parameters, comparatively, seems to play a relatively less important role, including wind direction. After wind forcing the model is most sensitive to bottom friction and wind direction. Nevertheless, the results of the analysis indicate that the selection of adequate bottom friction coefficients is fundamental for a good forecast.

To quantify the model capability of reproducing the observed water level, the statistics for the *optimal* case were computed (Table 2). The selection of the optimal set of parameters was the one that produced the minimum RMSE in both stations (Palermo and Oyarvide). It

TABLE 2. Statistical comparison between observed and simulated for the optimal case.

Station	RMSE (m)	R^2	P
Palermo	0.18	0.90	0.86
Oyarvide	0.16	0.85	0.90

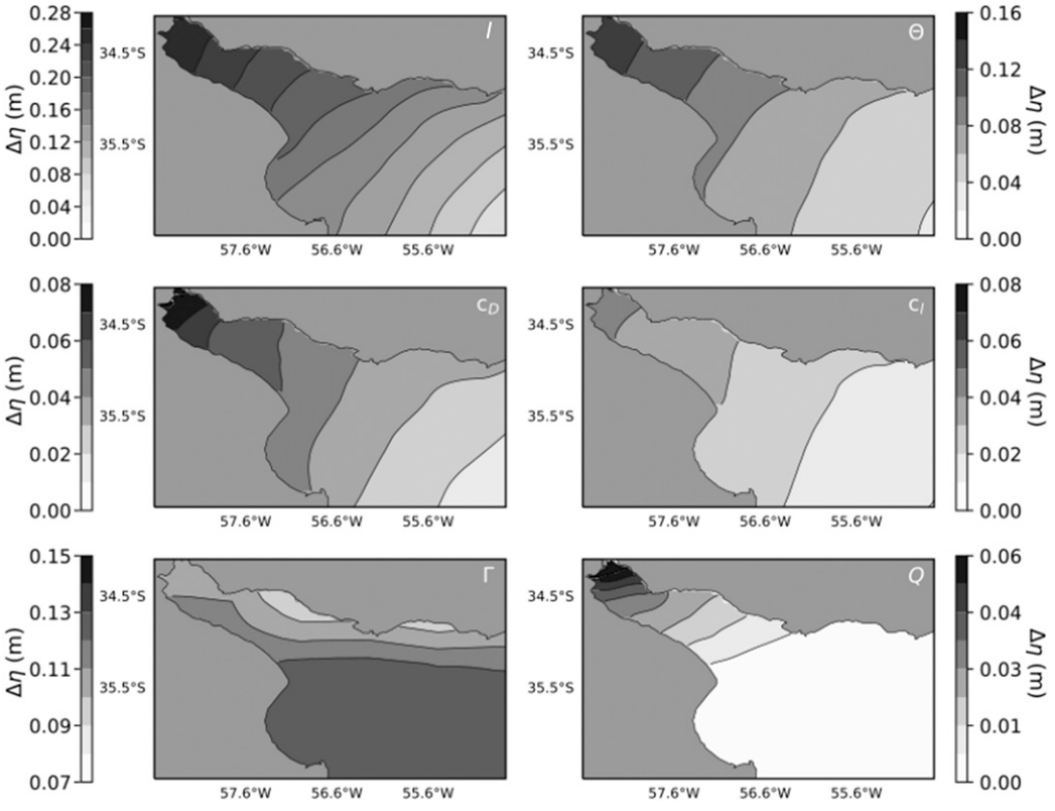

FIG. 5. Fields of the variation of the solution for extreme changes (from maximum to minimum) of each input $\Delta\eta$, keeping the others constant. The variation is expressed in terms of the root-mean-square differences (RMSD; m) between both solutions.

should be emphasized nevertheless that the selection of this set of parameters is not authentically optimal, but a first-order approximation that must be later refined, excluding from the analysis the less relevant parameters (setting them to the values suggested by the SA) and making a fine adjustment of the most important ones. RMSE indicates an overall error of 10%. The high determination coefficients (R^2), higher than 0.85, suggest a good timing in the reproduction of the storm surges. The linear regression slopes (P), lower than 0.9, highlight the need to carry out a wind speed improvement or adjustment, since for this optimal case $I = 1.20$ but the model solution still underestimates the water level. These results show that even though the model still needs a fine calibration or adjustment, the conclusions of the analysis can be regarded as valid.

b. *Implications for the modeling of water level*

The results of the Morris analysis indicate that the variability of all the inputs considered in the SA have a significant influence on the model solution for water level at the RdP estuary, as all of them are statistically different from zero. To quantify their relative effects, Fig. 5 shows the *fields of the variation of the solution* for extreme changes (from maximum to minimum) of each input $\Delta\eta$, keeping the others constant. The variation is expressed in terms of the root-mean-square difference (RMSD) between both solutions. This figure is useful in terms of better understanding the underlying processes and the impact of the input, but it does not provide information about the temporal evolution of the solution, particularly during the extreme events. As a complement, Fig. 6 shows the corresponding time series for Palermo station. The following inferences can be made from the figures:

- Wind speed I: From the physical point of view, it is the main forcing, as it is the source of energy for the generation of the surge. Therefore, it is natural to find that this is the parameter with maximum sensitivity; nevertheless, it must be also taken into account that it has large uncertainty. The spatial structure of the response to the wind (top panels of Fig. 5) is associated with the second mode of response of the estuary discussed by Simionato et al. (2004a; 2006) and in Fig. 3 of this paper, and increases upstream. For the

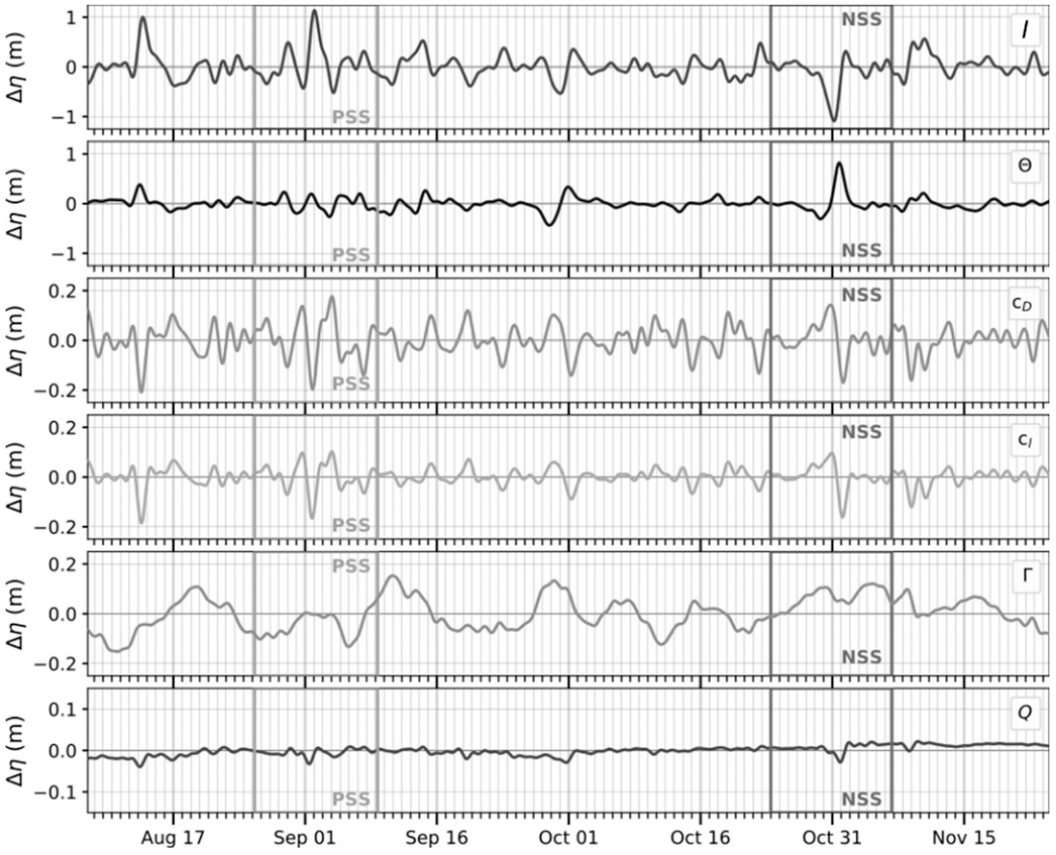

FIG. 6. Water level difference $\Delta\eta$ associated with the difference between the maximum and minimum values of every parameter considered for SA: wind speed w, wind direction Θ, bottom friction (c_D and c_l), atmospheric surface pressure gradient Γ, and continental discharge Q; in every case all the other parameters are kept constant. The boxes indicate the positive and negative storm surge (PSS and NSS, respectively) events.

moderate range of variability chosen for this input (±25%), the variability in the solution (top-left panel of Fig. 5) is large, with an RMSD of above 0.25 m for the whole period of simulation, even though it can be as large as 1.1 m during the surges at Palermo (located in the upper estuary). This way, an error in the wind speed will strongly propagate in the water level estimation for the RdP.

- Wind direction Θ: This parameter plays a role relatively less important than wind speed, at least for the considered range of ±15°. Figure 5 (top-right panel) shows that, however, this drives to an RMSD of approximately half of that due to changes in the wind speed (up to 0.15). The range of variability of the numerical solution associated with this parameter can reach 0.5 m at Palermo station (Fig. 6, for instance, for NSS), potentially driving a large error if the errors in wind direction are large. This is logical, as a large change in wind direction could force other of the modes of circulation of the estuary but not the surge.
- Bottom friction (c_D and c_l): These parameters regulate the amount of energy that is dissipated by bottom friction, and although this process occurs in nature, the impact it has on reducing the surge at the RdP is relatively low. Changes in the surge associated with changes in this input increase upstream as a result of the reduction in water level (center panel of Fig. 5). On the other hand, note that the spatial pattern is more asymmetrical than that related to the wind, slightly increasing to the south; this is consistent with the knowledge that tidal energy is dissipated there (Simionato et al. 2005). The RMSD is about 0.08 m, one-third of that associated with wind speed, and half of the related to wind direction. Figure 6 (third and fourth panels) shows that, for the large range of variation chosen for the bottom friction parameters, the range of variability of the water level numerical solutions at Palermo station is of the order of 0.2 m. This might seem small, but it must be taken into account that it represents an error of around 10% and that, therefore, it is significant.

- Atmospheric surface pressure gradient Γ: The spatial distribution of the difference of the simulations considering and not considering this input (bottom-left panel of Fig. 5) follows the expected pattern, related to the presence of a semipermanent low over Uruguay (Seluchi and Saulo 1998), improving in this way the solution particularly in the northern part of the domain. In general, the effect is significant all over the estuary, with an RMSD of up to 0.15 m. The atmospheric surface pressure gradient Γ reaches variations of that order at Palermo station (fifth panel in Fig. 6). It should be kept in mind that sea level pressure is actually well determined by atmospheric models and that, therefore, the associated *error* would occur more if the Γ is not incorporated in the simulations than as a result of errors in the estimation of that variable.
- Continental discharge Q: The spatial distribution of the effect of this input (bottom-right panel of Fig. 5) naturally resembles the pattern of the freshwater plume under the Coriolis force in the Southern Hemisphere (Simionato et al. 2004a). Results indicate that, in spite of the huge runoff of the RdP, the effect of the continental discharge on water level is relatively weak, with an RMSD of up to 0.06 m. This result seems to be related with the estuary scale; although the considered runoff variations are large (±50%), the RdP is very wide and the mean current due to the runoff is much weaker than the speed of the huge water mass mobilized during the surge; also the amount of rainfall during these storms in the RdP is very small compared to the huge mean runoff of this estuary. It is worthwhile to note that this is not the case in other estuarine systems of the world (e.g., Herdman et al. 2018; Pietrafesa et al. 2019). Also, it should be considered that the errors in the determination of this variable are small, as good quality measurements are made by the National Institute for Water of Argentina (Borús et al. 2006). Therefore, only a small error can be expected as a result errors in this input. Note that at Palermo station the variation (lower panel of Fig. 6) is quite homogeneous in time due to the fact that the runoff does not change along a particular simulation. Nevertheless, the changes during the surges suggest that nonlinear interactions between the surge and the runoff might be occurring.

From the practical point of view the above results highlight to some needs for the construction of a reliable water level hindcast/forecast system for the RdP:

1) It is necessary to make a good adjustment of the bottom friction parameters; nevertheless, as the effect of uncertainties on those inputs are relatively small, it is probably enough to choose the values that produce the optimal solution of the SA.
2) It is highly advisable to incorporate the atmospheric surface pressure gradient in the surge simulation; otherwise errors in the estimation can be as large as 0.15 m.
3) Even though it is advisable to include the runoff in simulations oriented on short-range or medium-range forecasting, small errors in the continental discharge cannot be regarded as a first-order effect on forecasting errors. This is quite fortunate, because the forecast of the runoff demands hydrological modeling, adding a complex practical issue for forecast purposes. In this sense, and due to the long scales of variability (mostly interannual) of this input compared to the scale of hours of the surge, the use of the discharge measured a few days ago as forcing of the forecast surge model would be enough for practical purposes. In other words, the hydrological modeling of the runoff can be decoupled from the hydrodynamical modeling of the surge for practical surge forecast purposes.
4) It is absolutely necessary to select a good quality wind forcing, both speed and direction, in the simulations, because the error associated with even small changes in these inputs can become large errors in the estimation of the surge. As it will be discussed in what follows, the uncertainties in this variable will become the main source of uncertainty in the forecast/hindcast that must be estimated somehow to provide valuable information to users.

c. *Wind uncertainty*

Even though the aspects 1–3, discussed above, are relatively easy to implement in the numerical modeling system, the last point can become a difficult issue in practice. To illustrate the problem of the selection of the wind field, a comparison between direct observations and wind reanalyses at the region of interest is shown in Fig. 7. The figure was built for the same period of the SA, when direct wind observations (dots in Fig. 7) were collected at an oceanographic buoy that was deployed at 35.2°S, 56.4°W (square in Fig. 1). In addition, the Taylor diagram associated with the wind speed is shown for a statistical comparison (Fig. 7, top-right panel). Four different wind reanalyses are shown with the aim of considering (i) the potential differences and improvements in the diverse models' physics, parameterizations, and assimilation schemes, and (ii) the temporal and spatial resolution of the reanalysis models. They are as follows:

- ERA-Interim (ERAI, dark blue): 6-hourly reanalysis from the European Centre for Medium-Range Weather Forecast, with 0.75° spatial resolution (Dee et al. 2011).
- ERA5 (brown): 1-hourly reanalysis from the European Centre for Medium Range Weather Forecast, with

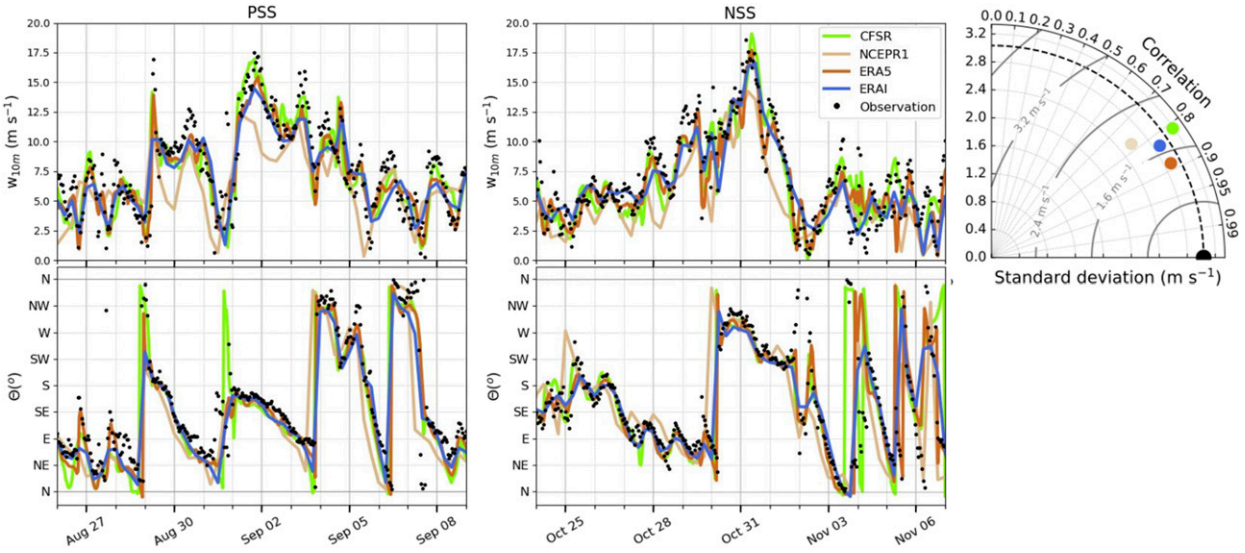

FIG. 7. Comparison of (top) wind speed at 10 m and (bottom) wind direction among direct observation (black dots) and four atmospheric reanalyses: ERA Interim (ERAI, dark blue), ERA5 (brown), NCEP/NCAR RI (NCEPR1, beige), and CFSR (green). The periods shown correspond to the (left) positive storm surge (PSS) and (center) negative storm surge (NSS) events. (right) The Taylor diagram associated with the wind speed; this diagram was built for the period between December 2009 and December 2010.

0.25° spatial resolution (Copernicus Climate Change Service C3S 2017).

- NCEP–NCAR RI (NCEPR1, beige): 6-hourly reanalysis from the NOAA/National Centers for Environmental Prediction–National Center for Atmospheric Research, with 1.875° spatial resolution (Kalnay et al. 1996).
- CFSR (green): 1-hourly reanalysis from Climate Forecast System Reanalysis of NCAR/UCAR, with 0.25° spatial resolution (National Center for Atmospheric Research 2017).

Figure 7 shows that there is a large dispersion among the diverse reanalysis models, even those that come from the same forecast center (ERAI/ERA5 and NCEPR1/CFSR). Although some reanalyses seem to offer better estimations of the wind than others, the result strongly depends upon the selected period and on the variability during this period. This dependence becomes more obvious when longer periods of time (not shown) are considered. In addition, whereas some reanalyses seem to be more accurate for wind speed, others make a better estimation of the time of the peak of the storm or of the wind direction. For instance, on 29 August ERA5 and CFSR present good estimations of the wind direction but both underestimate the wind speed. The inherent uncertainty in the actual values of the atmospheric input (wind speed and direction, and to a lesser extent sea surface pressure), raise the question of how large is their combined impact on the uncertainty of the water level model solution.

To provide a first-order estimation of the impact of uncertainties in the atmospheric fields due to the selection of the inputs, a set of different water level solutions forced by the four above mentioned reanalyses was carried out (Fig. 8). The same period of time (1 August–1 December) was simulated setting $c_l = 1 \times 10^{-4}\,\mathrm{m\,s^{-1}}$ and $c_D = 2 \times 10^{-3}$ (optimal values from the SA), Q was set to the observed values; wind speed and direction and sea level pressure were used as they are provided by the forecast centers, without any adjustment or calibration. Figure 8 shows the set of numerical solutions for the storm surge extreme events (PSS at right and NSS at center) at Palermo. Direct observations are in black, whereas the mean of the set is in red and the shade represents the dispersion among solutions measured as the range between the minimum and the maximum value estimated for every instant. The right panel of the figure displays the Taylor diagram (Taylor 2001) for the full period of analysis. The Taylor diagram shows that even though there are large differences in the atmospheric forcing among reanalyses (Fig. 7), the surge numerical solutions present similar correlations and only slightly different standard deviations. This indicates that the reanalyses have a better representation of the wind evolution in time than of wind speed. Statistically, it means that the reanalyses yield solutions with high correlations with the observations but with linear regression slopes that departure from 1. Large spreading in the amplitude of the signal is observed for both extreme events, with a mean signal that underestimates the observations in all the cases. Moreover, it is necessary to take into account a wide spreading to keep the observation within the hindcast. Also, the spreading becomes larger during the peaks of the surges.

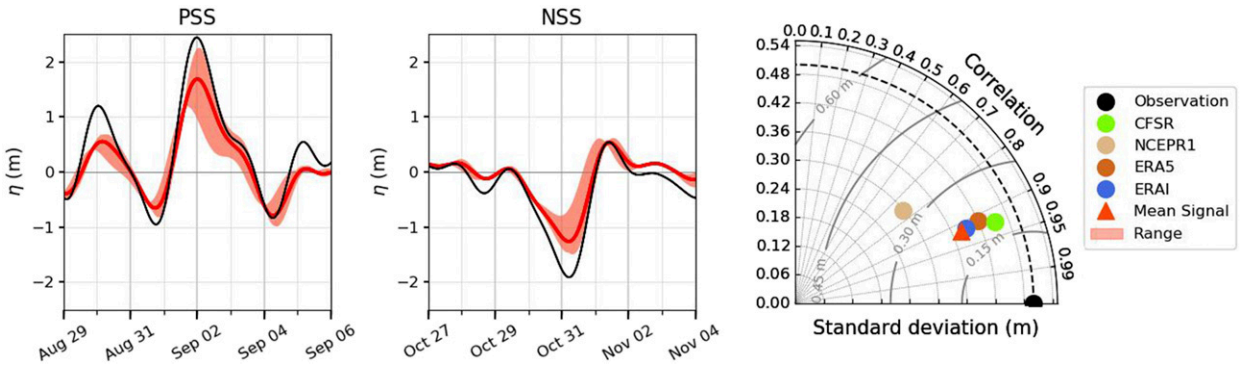

FIG. 8. Comparision between direct storm surge observations (black line) and the spectrum of solutions forcing with the four atmospheric reanalyses: mean solution (red line) and range of the solutions (shadow). The comparison for the (left) positive storm surge (PSS), (center) negative storm surge (NSS), and (right) the respective Taylor diagram for the full period.

Even perhaps exacerbated by the fact that some reanalyses are clearly worse for this area than others, Fig. 8 illustrates how the uncertainty in the atmospheric forcing can drive large errors in the storm surge amplitude hindcast in the RdP. For the particular case of the chosen reanalyses and periods, the amplitude of the modeled surge can be half of the observed one. From the point of view of the applications, this error is not only very large, but can make the difference between hindcasting (and eventually forecasting) an emergency or not. During the revision process, the question arose if the result shown in Fig. 8 could derive from the fact that NCEP seems to behave differently than the other reanalysis, particularly underestimating more strongly the wind speed. Nevertheless, the uncertainty in the solution still occurs if that reanalysis is not considered, and it is magnified during surges, with differences of up to 0.5 m for PSS. The problem of the uncertainties in the atmospheric fields increases for the forecasts. The atmospheric forecast models are less constrained by observations (they are only assimilated in the initial condition) than the reanalyses and, therefore, errors and uncertainties grow. In consequence, the forecast centers usually do not provide a single estimation of future values but give a measurement of the uncertainty through ensemble modeling. The above discussion suggests that that dispersion should be taken into account in numerical modeling of water level at the RdP to provide the users with useful estimations.

4. Conclusions and recommendations

In this work, the CROCO model was chosen as the base to build a regional application for hindcast (and eventually forecast) of water level in the northern Argentinean (southwestern Atlantic) continental shelf with emphasis in the large, wide, and fast-flowing Río de la Plata (RdP) estuary. The model code was modified to include the atmospheric surface pressure, variable continental runoff, and tides in 2D. It was then applied in a hierarchy of one-way nested grids with refinement of the solutions over the RdP.

For the first time, a sensitivity analysis (SA; based on the Morris method) was applied to this region to determine the sensitivity of numerical solutions to uncertainties on the different model inputs (parameters and forcings) and/or to evaluate the need of their inclusion in the model for a proper hindcasting/forecasting. The SA included the bottom friction quadratic and linear parameterizations, the wind forcing (wind speed and direction), the atmospheric surface pressure, and the continental discharge. The results of the analysis provide information that allows for a relatively cheap and objective first calibration of the model and that permits a future optimal calibration with only a fine tuning and a minimum number of simulations. They also allow for a better understanding of the impact of the physical processes that force the surge and highlight the needs to face the construction of an appropriate numerical hindcast/forecast system for the estimation of water level and, in particular extreme surges, in the RdP. In particular, our work is the first one that applyes a mathematical technique to formalize aspects that are accepted more than understood for the region, occasionally wrongly, emphasizing the need for further studies regarding forecast uncertainty in water level and extreme surge due to errors in forecast wind speed.

The SA showed that the most important aspect for a successful estimation of the surge amplitude and timing is the selection of a good quality atmospheric forcing, especially wind speed and direction, because the error associated with even small uncertainties in these inputs can become large errors in the estimation of the surge. This leads to a substantial practical problem, as winds

from diverse sources show large differences among them. Results also show that an appropriate surge modeling system for the RdP requires a good adjustment of the bottom friction parameters; that it is advisable to incorporate the atmospheric surface pressure gradient effect in the surge simulation; and that the discharge must be included in the simulations but, due to the scales of variability of the runoff in this basin, a small error in the estimation of discharge will not seriously affect the results of the level forecast. This way, from a practical point of view, hydrological modeling of runoff can be decoupled of the hydrodynamical modeling of the surge in this estuary, in spite of its enormous discharge.

A comparison of the storm surges simulated with different reanalyses provided by the most important forecast centers of the world, show that model hindcasts can fail in the estimation of the surge amplitude in up to 50%. It can be expected that this problem will increase when forecast instead of hindcast is faced, as forecast atmospheric models are less constrained by observations than reanalysis models. The fact that the surge models are so sensitive even to small uncertainties in the winds raises an important practical problem in a region like the RdP, where direct atmospheric observations are scarce. In particular, how can surge forecasts be improved and how can users be provided with useful information that can be properly assessed and decisions made accordingly?

The most obvious way of improving the surge estimation would be either improving the atmospheric forcing or at least quantifying the hindcast/forecast error due to the inherent uncertainties. Some ways of improving the wind forcing is by increasing the diversity of physical processes included in the simulations (and, if needed, the temporal and spatial resolution), by the use of atmospheric regional numerical models and/or assimilating more data in the simulations. For this, more atmospheric direct observations over the Southern Hemisphere and particularly over the RdP region would be necessary; the problem becomes more complex due to the fact that in this area even remote observations have limitations due to the proximity of the coast. As an intermediate step, an empirical adjustment of the winds should be attempted.

Due to the above mentioned difficulties regarding winds in the area, the wind forcing will remain, therefore, a significant source of errors and uncertainties for any surge hindcast/forecast model for the region in the near future. To provide users with better information, uncertainties in the water level estimations should be quantified, for instance, by ensemble modeling. In this sense, it is foreseen that it will be the next step in the development of this application. Also, retrospective studies using actual forecast meteorology to develop an understanding of the increased error using forecast *versus* reanalysis meteorology would be advisable.

Acknowledgments. This study was funded by the National Agency for Scientific and Technological Research of Argentina (ANPCyT) PICT 2014-2672 Project, the Programa de Investigación y Desarrollo para la Defensa del MINDEF (PIDDEF) 14-14 Project, and the UBACYT 20020150100118BA directed by Claudia G. Simionato. Matías G. Dinapoli's participation was possible thanks to an ANPCyT PhD fellowship.

REFERENCES

Balay, M. A., 1961: El Río de la Plata entre la atmósfera y el mar. Publicación H-621, Buenos Aires: Servicio de Hidrografía Naval, Armada Argentina, 153 pp.

Bastidas, L., J. Knighton, and S. Kline, 2016: Parameter sensitivity and uncertainty analysis for a storm surge and wave model. *Nat. Hazards Earth Syst. Sci.*, **16**, 2195–2210, https://doi.org/10.5194/nhess-16-2195-2016.

Borús, J., M. U. Quirno, and D. Calvo, 2006: Evaluación de caudales diarios descargados por los grandes riós del sistema del Plata al estuario del Río de la Plata. *Dirección de Sistemas de Información y Alerta Hidrológico*, Instituto Nacional del Agua, 154 pp.

Bowden, K. F., 1983: *Physical Oceanography of Coastal Waters*. E. Horwood, 302 pp.

Campolongo, F., J. Cariboni, and A. Saltelli, 2007: An effective screening design for sensitivity analysis of large models. *Environ. Modell. Software*, **22**, 1509–1518, https://doi.org/10.1016/J.ENVSOFT.2006.10.004.

Combes, V., and R. Matano, 2014: A two-way nested simulation of the oceanic circulation in the southwestern Atlantic. *J. Geophys. Res. Oceans*, **119**, 731–756, https://doi.org/10.1002/2013JC009498.

——, and ——, 2019: On the origins of the low-frequency sea surface height variability of the Patagonia shelf region. *Ocean Modell.*, **142**, 101454, https://doi.org/10.1016/j.ocemod.2019.101454.

Copernicus Climate Change Service C3S, 2017: ERA5: Fifth generation of ECMWF atmospheric reanalyses of the global climate. Copernicus Climate Change Service Climate Data Store (CDS), accessed 4 May 2020, https://cds.climate.copernicus.eu/#!/home.

Courant, R., K. Friedrichs, and H. Lewy, 1928: Uber die partiellen differenzengleichungen der mathematischen physik. *Math. Ann.*, **100**, 32–74, https://doi.org/10.1007/BF01448839.

Debreu, L., P. Marchesiello, P. Penven, and G. Cambon, 2012: Two-way nesting in split-explicit ocean models: Algorithms, implementation and validation. *Ocean Modell.*, **49–50**, 1–21, https://doi.org/10.1016/j.ocemod.2012.03.003.

Dee, D. S., and Coauthors, 2011: The ERA-Interim reanalysis: Configuration and performance of the data assimilation system. *Quart. J. Roy. Meteor. Soc.*, **137**, 553–597, https://doi.org/10.1002/qj.828.

Diario-Clarín, 2010: Sudestada: 1.400 evacuados por la peor crecida en 10 anos. Diario Clarín, accessed 4 May 2020, https://www.clarin.com/capital_federal/Sudestada-evacuados-peor-crecida-anos_0_HJM566P7e.html.

——, 2012: SIGUE EL MAL TIEMPO: Tras la sudestada, cesó el alerta por vientos fuertes. Diario Clarín, accessed 4 May 2020,

https://www.clarin.com/sociedad/alerta-inundaciones-zona-costera-sudestada_0_r16mStyhD7e.html.

Dinápoli, M., 2016: Estudio de la sensibilidad de un modelo barotrópico 2D para la predicción del nivel del mar. M.S. thesis, Facultad de Ciencias Exactas y Naturales, Universidad de Buenos Aires, 92 pp.

D'Onofrio, E., M. Fiore, and S. Romero, 1999: Return periods of extreme water levels estimated for some vulnerable areas of Buenos Aires. *Cont. Shelf Res.*, **19**, 1681–1693, https://doi.org/10.1016/S0278-4343(98)00115-0.

——, ——, and J. L. Pousa, 2008: Changes in the regime of storm surges at Buenos Aires, Argentina. *J. Coastal Res.*, **1**, 260–265, https://doi.org/10.2112/05-0588.1.

——, F. Oreiro, and M. Fiore, 2012: Simplified empirical astronomical tide model—An application for the Río de la Plata estuary. *Comput. Geosci.*, **44**, 196–202, https://doi.org/10.1016/j.cageo.2011.09.019.

Ferreira, C., J. Irish, and F. Olivera, 2014: Uncertainty in hurricane surge simulation due to land cover specification. *J. Geophys. Res. Oceans*, **119**, 1812–1827, https://doi.org/10.1002/2013JC009604.

Framinan, M., M. Etala, E. Acha, R. Guerrero, C. Lasta, and O. Brown, 1999: Physical characteristics and processes of the Río de la Plata Estuary. *Estuaries of South America: Their Geomorphology and Dynamics*, G. M.E. Perillo, M. C. Piccolo, and M. Pino-Quivira, Eds., Springer, 161–194.

Gan, M., and V. Rao, 1991: Surface cyclogenesis over South America. *Mon. Wea. Rev.*, **119**, 1293–1302, https://doi.org/10.1175/1520-0493(1991)119<1293:SCOSA>2.0.CO;2.

Gary, D., and S. Y. Erofeeva, 2002: Efficient inverse modeling of barotropic ocean tides. *J. Atmos. Oceanic Technol.*, **19**, 183–204, https://doi.org/10.1175/1520-0426(2002)019%3C0183:EIMOBO%3E2.0.CO;2.

Gayathri, R., P. K. Bhaskaran, and P. Murty, 2019: River-tide-storm surge interaction characteristics for the Hooghly estuary, East coast of India. *ISH J. Hydraul. Eng.*, https://doi.org/10.1080/09715010.2019.1601036, in press.

Gill, A. E., 1982: *Atmosphere–Ocean Dynamics*. Academic Press, 662 pp.

Herdman, L., L. Erikson, and P. Barnard, 2018: Storm surge propagation and flooding in small tidal rivers during events of mixed coastal and fluvial influence. *J. Mar. Sci. Eng.*, **6**, 158, https://doi.org/10.3390/jmse6040158.

Höllt, T., M. U. Altaf, K. T. Mandli, M. Hadwiger, C. N. Dawson, and I. Hoteit, 2015: Visualizing uncertainties in a storm surge ensemble data assimilation and forecasting system. *Nat. Hazards*, **77**, 317–336, https://doi.org/10.1007/s11069-015-1596-y.

Hoyer, S., and J. Hamman, 2017: Xarray: N-D labeled arrays and datasets in python. *J. Open Res. Software*, **5**, 10, https://doi.org/10.5334/jors.148.

Idier, D., F. Dumas, and H. Muller, 2012: Tide-surge interaction in the English channel. *Nat. Hazards Earth Syst. Sci.*, **12**, 3709–3718, https://doi.org/10.5194/nhess-12-3709-2012.

Jaime, P., A. Menéndez, M. U. Quirno, and J. Torchio, 2002: Análisis del régimen hidrológico de los ríos Paraná y Uruguay. Informe LHA 05-216-02, Instituto Nacional del Agua, Buenos Aires, Argentina, 69 pp.

Kalnay, E., 2002: *Atmospheric Modeling, Data Assimilation and Predictability*. Cambridge University Press, 341 pp.

——, and Coauthors, 1996: The NCEP/NCAR 40-Year Reanalysis Project. *Bull. Amer. Meteor. Soc.*, **77**, 437–471, https://doi.org/10.1175/1520-0477(1996)077<0437:TNYRP>2.0.CO;2.

Kresning, B., M. R. Hashemi, S. P. Neill, J. A. M. Green, and H. Xue, 2019: The impacts of tidal energy development and sea-level rise in the Gulf of Maine. *Energy*, **187**, 115942, https://doi.org/10.1016/J.ENERGY.2019.115942.

Luz Clara, M., C. Simionato, E. D'Onofrio, M. Fiore, and D. Moreira, 2014: Variability of tidal constants in the Río de la Plata estuary associated to the natural cycles of the runoff. *Estuarine Coastal Shelf Sci.*, **148**, 85–96, https://doi.org/10.1016/J.ECSS.2014.07.002.

Mayo, T., T. Butler, C. Dawson, and I. Hoteit, 2014: Data assimilation within the advanced circulation (ADCIRC) modeling framework for the estimation of Manning's friction coefficient. *Ocean Modell.*, **76**, 43–58, https://doi.org/10.1016/j.ocemod.2014.01.001.

Meccia, V., C. Simionato, M. Fiore, E. D'Onofrio, and W. Dragani, 2009: Sea surface height variability in the Río de la Plata estuary from synoptic to inter-annual scales: Results of numerical simulations. *Estuarine Coastal Shelf Sci.*, **85**, 327–343, https://doi.org/10.1016/j.ecss.2009.08.024.

Met Office, 2015: Cartopy: A cartographic python library with a matplotlib interface. Met Office, accessed 4 May 2020, https://scitools.org.uk/cartopy/docs/latest/.

Morris, M., 1991: Factorial sampling plans for preliminary computational experiments. *Technometrics*, **33**, 161–174, https://doi.org/10.1080/00401706.1991.10484804.

National Center for Atmospheric Research, 2017: The Climate Data Guide: Climate Forecast System Reanalysis (CFSR). Copernicus Climate Change Service Climate Data Store (CDS), accessed 4 May 2020, https://climatedataguide.ucar.edu/climate-data/climate-forecast-system-reanalysis-cfsr.

NOAA, 2006: 2-minute Gridded Global Relief Data (ETOPO2) v2. National Geophysical Data Center, NOAA, accessed 4 May 2020, https://doi.org/10.7289/V5J1012Q.

Norton, J., 2015: An introduction to sensitivity assessment of simulation models. *Environ. Modell. Software*, **69**, 166–174, https://doi.org/10.1016/j.envsoft.2015.03.020.

Pedlosky, J., 1987: *Geophysical Fluid Dynamics*. 2nd ed. Springer-Verlag, 710 pp.

Pietrafesa, L., H. Zhang, S. Bao, P. Gayes, and J. Hallstrom, 2019: Coastal flooding and inundation and inland flooding due to downstream blocking. *J. Mar. Sci. Eng.*, **7**, 336, https://doi.org/10.3390/jmse7100336.

Powell, M., P. Vickery, and T. Reinhold, 2003: Reduced drag coefficient for high wind speeds in tropical cyclones. *Nature*, **422**, 279–283, https://doi.org/10.1038/nature01481.

Pugh, D., 2004: *Changing Sea Levels: Effects of Tides, Weather and Climate*. Cambridge University Press, 265 pp.

Robertson, A., and C. Mechoso, 1998: Inter-annual and decadal cycles in river flows of southeastern South America. *J. Climate*, **11**, 2570–2581, https://doi.org/10.1175/1520-0442(1998)011<2570:IADCIR>2.0.CO;2.

ROMS, 2005: Regional Ocean Modeling System. Accessed 4 May 2020, https://www.myroms.org/.

Sakamoto, K., H. Tsujino, H. Nakano, S. Urakawa, T. Toyoda, N. Hirose, N. Usui, and G. Yamanaka, 2019: Development of a 2-km resolution ocean model covering the coastal seas around Japan for operational application. *Ocean Dyn.*, **69**, 1181–1202, https://doi.org/10.1007/S10236-019-01291-1.

Santoro, P., M. Fernández, M. Fossati, G. Cazes, R. Terra, and I. Piedra-Cueva, 2011: Pre-operational forecasting of sea level height for the Río de la Plata. *Appl. Math. Model.*, **35**, 2462–2478, https://doi.org/10.1016/j.apm.2010.11.065.

Saraceno, M., E. D'Onofrio, M. Fiore, and W. Grismeyer, 2010: Tide model comparison over the southwestern Atlantic shelf. *Cont. Shelf Res.*, **30**, 1865–1875, https://doi.org/10.1016/j.csr.2010.08.014.

Seluchi, M. E., and A. C. Saulo, 1998: Possible mechanisms yielding an explosive coastal cyclogenesis over South America: Experiments using a limited area model. *Aust. Meteor. Mag.*, **47**, 309–320.

Shchepetkin, A. F., and J. C. McWilliams, 2005: The Regional Oceanic Modeling System (ROMS): A split-explicit, free-surface, topography-following-coordinate oceanic model. *Ocean Modell.*, **9**, 347–404, https://doi.org/10.1016/j.ocemod.2004.08.002.

Shiklomanov, I. A., 1998: A summary of the monograph world water resources. *World Water Resources: A New Appraisal and Assessment for the 21st Century*, UNEP: Society and Cultural Organization, 37 pp, https://unesdoc.unesco.org/ark:/48223/pf0000112671.

SHN, 1986: Mar Argentino, de Río de la Plata al Cabo de Hornos, Carta Náutica 50. 4th ed. Servicio de Hidrografía Naval, Armada Argentina.

——, 1992: Acceso al Río de la Plata, Carta Náutica H1. 5th ed. Servicio de Hidrografía Naval, Armada Argentina.

——, 1993: El Rincón, Golfo San Matías y Nuevo, Carta Náutica H2. 4th ed. Servicio de Hidrografía Naval, Armada Argentina.

——, 1999a: Río de la Plata Medio y Superior, Carta Náutica H116. 4th ed. Servicio de Hidrografía Naval, Armada Argentina.

——, 1999b: Río de la Plata Exterior, Carta Náutica H113. 2nd ed. Servicio de Hidrografía Naval, Armada Argentina.

Simionato, C. G., W. Dragani, V. Meccia, and M. Nuñez, 2004a: A numerical study of the barotropic circulation of the Río de la Plata estuary: Sensitivity to bathymetry, the earth's rotation and low frequency wind variability. *Estuarine Coastal Shelf Sci.*, **61**, 261–273, https://doi.org/10.1016/j.ecss.2004.05.005.

——, ——, M. Nuñez, and M. Engel, 2004b: A set of 3-D nested models for tidal propagation from the Argentinian continental shelf to the Río de la Plata estuary—Part I: M2. *J. Coastal Res.*, **203**, 893–912, https://doi.org/10.2112/1551-5036(2004)20[893:ASODNM]2.0.CO;2.

——, V. Meccia, W. Dragani, and M. Nuñez, 2005: Barotropic tide and baroclinic waves observations in the Río de la Plata Estuary. *J. Geophys. Res.*, **110**, C06008, https://doi.org/10.1029/2004JC002842.

——, V. L. Meccia, W. C. Dragani, and M. N. Nuñez, 2006: On the use of the NCEP/NCAR surface winds for modeling barotropic circulation in the Río de la Plata Estuary. *Estuarine Coastal Shelf Sci.*, **70**, 195–206, https://doi.org/10.1016/j.ecss.2006.05.047.

Taylor, K. E., 2001: Summarizing multiple aspects of model performance in a single diagram. *J. Geophys. Res.*, **106**, 7183–7192, https://doi.org/10.1029/2000JD900719.

WMO, 2011: Guide to storm surge forecasting. WMO Tech. Rep. WMO-1076, World Meteorological Organization, 120 pp., http://hdl.handle.net/11329/393.

Wolf, J., 1978: Interaction of tide and surge in a semi-infinite uniform channel, with application to surge propagation down the east coast of Britain. *Appl. Math. Model.*, **2**, 245–253, https://doi.org/10.1016/0307-904X(78)90017-3.

Zhang, W.-Z, F. Shi, H.-S Hong, S.-P Shang, and J. T. Kirby, 2010: Tide-surge interaction intensified by the Taiwan strait. *J. Geophys. Res.*, **115**, C06012, https://doi.org/10.1029/2009JC005762.